AD-A068 420 RENSSELAER POLYTECHNIC INST TROY N Y COMMUNICATION A--ETC F/G 9/4
IMAGE ENHANCEMENT BY STOCHASTIC HOMOMORPHIC FILTERING.(U)
FEB 79 R W FRIES, J W MODESTINO N00014-75-C-0281
UNCLASSIFIED TR-79-2 NL

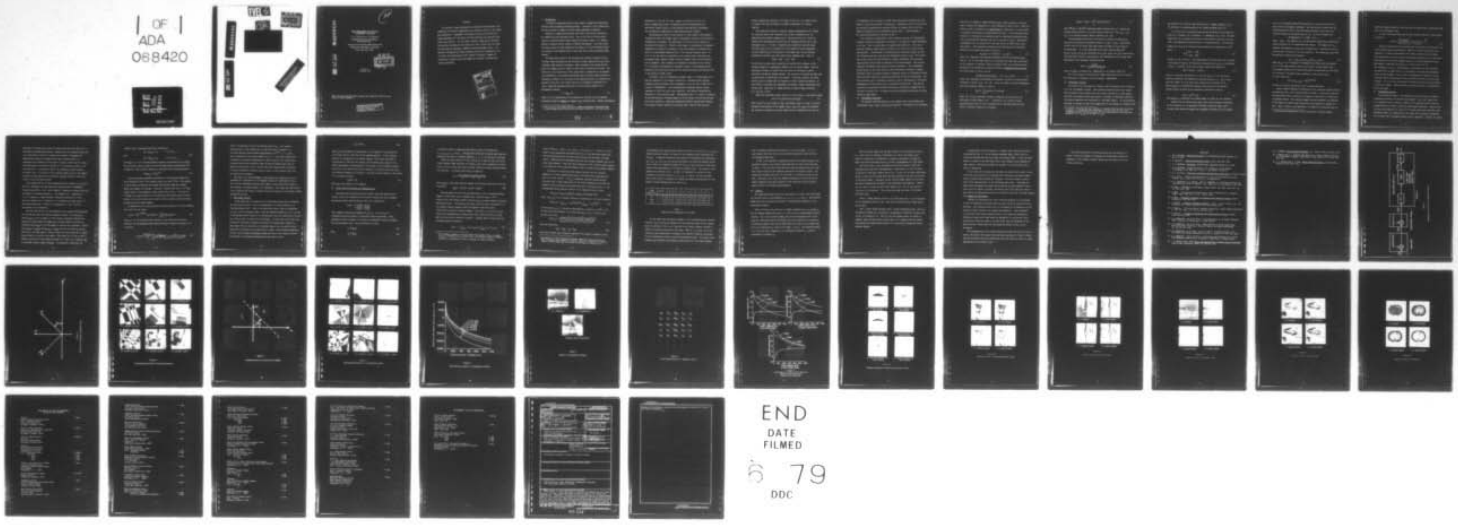

END
DATE FILMED
6 79
DDC

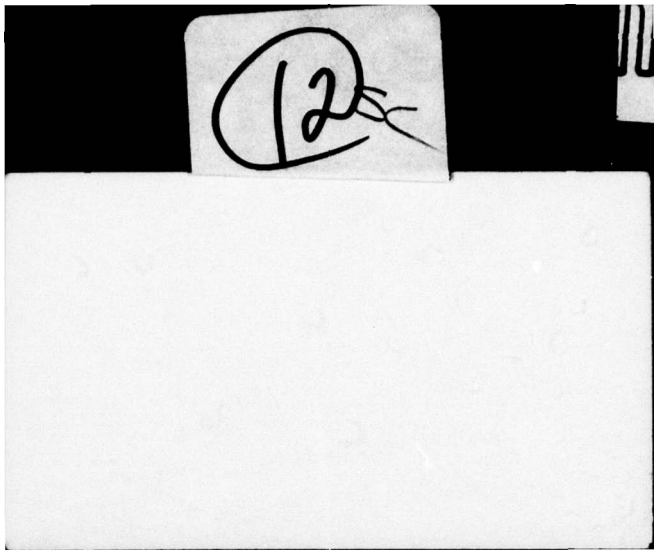
12

Image Enhancement by Stochastic Homomorphic Filtering

R. W. Fries and J. W. Modestino

Communications and Information Processing Group

Electrical and Systems Engineering Dept.

Rensselaer Polytechnic Institute

Troy, New York 12181

TR 79-2
February 1979

This work was performed under Contract No. N00014-75-C-0281 for the Office of Naval Research

Abstract

The problem of image enhancement by nonlinear two-dimensional (2-D) homomorphic filtering is approached using stochastic models of the signal and degradations. Homomorphic filtering has been used previously for image enhancement but the linear filtering operation has generally been chosen heuristically. In this paper stochastic image models described and analyzed previously by the authors are used to model the true image and interferring components (shadows and salt-and-pepper noise). The problem of designing the linear operation can then be formulated as one of linear least mean-squared error (Wiener) filtering. Examples of processing on typical real-world images are included to indicate the results obtainable.

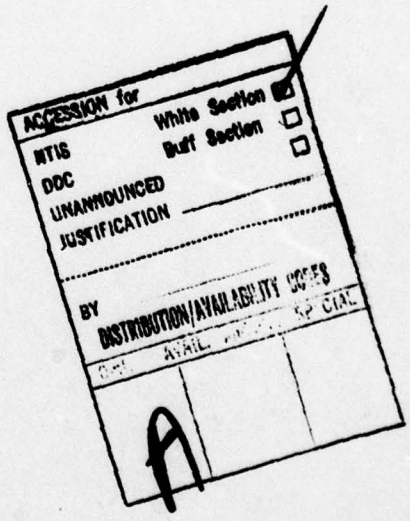

I. Introduction:

A problem in representing data in any format is emphasizing significant features while minimizing distracting detail. Solutions of this problem when the data consists of images are called image enhancement techniques.

Elements in images which distract the viewer from relevant information are shadows and salt-and-pepper noise. This is the case for either photochemical or photoelectronic image sensing and display systems. For example, shadows frequently obscure detail in ordinary photographs; even when detail is present within the area darkened by the shadow it is often subdued because the contrast in the darkened area is less than that in the surrounding bright regions.†

The same effect occurs in the recording and display of images by photoelectronic means although here the problem is further aggravated by the limited dynamic range generally available. Many TV monitors and storage CRT displays, for example, are not capable of more than 32 distinct gray levels. The severity of this restriction is best appreciated in comparison to the capabilities afforded by a good quality photograph under subjective human evaluation. According to Zoethout [1], the ratio of the smallest variation in intensity discernible by the eye to the overall intensity is generally considered to be 1/100. Using the standard definition [2] of the optical density D of a photographic emulsion

$$D = \log_{10} 1/T \quad , \tag{1}$$

where T is the transmittance of the emulsion, we conclude that the smallest discernible change in density is roughly $\log_{10} 101/100 = 0.0043$. Typical photographic

† This is due to the common practice in modern photography of exposing film so that shadows fall on the toe of the D-log E curve (cf. [19], pp. 29-32).

emulsions (cf. [2], pg. 69) cover a range of densities from 0 to 1.5. Hence, assuming grain noise is negligible there are approximately 347 discernible density levels in a good quality black-and-white photograph; far exceeding the capabilities of most photoelectronic displays.

The mechanism by which the eye achieves its wide dynamic range suggests techniques by which the dynamic range of photographic materials and electronic displays may be extended. The sensitivity of the eye to local changes is described by Hochberg [3]. Within a broad range of illuminations the apparent brightness of a region is a function of the ratio between its intensity and that of its surrounding region and not of its absolute intensity alone. It is as if the eye takes the logarithm of the incoming light intensities and then passes these signals through a spatial highpass filter which attenuates the DC component. This contention is supported by Stockham [4] who carries it to the point of estimating the frequency response of the highpass filter. Additional work along these lines has been provided by Mannos and Sakrison [20] in the context of image coding.

One method, then, of extending the dynamic range of recorded images is to take the logarithm of the original intensities; attenuate slowly varying components which contribute little information to the eye (and, indeed act as a source of degradation) while simultaneously enhancing rapidly varying components to which the eye is most sensitive; and finally, presenting the exponential of the processed image. Photographers have, to a degree, accomplished this processing in recording images on film by using a fast-acting developer with little agitation; exhausted chemicals from heavily exposed areas diffuse into adjacent lightly exposed areas causing them to develop even less and

thereby emphasizing transitions from light to dark [2]. For images stored in digital form this processing is readily accomplished by a digital computer.

This paper then describes a specific digital implementation of a scheme for enhancing rapid local variations due to object boundaries and de-emphasizing more gradual changes such as those which occur as a result of shadows while simultaneously controlling the degrading effects due to salt-and-pepper noise. In order to formulate this problem the observed image intensity $s_0(\underline{x})$ will be considered to be the product of three components: the true reflectivity of the objects in the image $r(\underline{x})$, the non-constant illumination function $i(\underline{x})$, and a white noise component $n(\underline{x})$. That is,

$$s_0(\underline{x}) = r(\underline{x}) \cdot i(\underline{x}) \cdot n(\underline{x}) \quad . \tag{2}$$

We note that the noise here is modeled as a multiplicative process in the intensity domain or, equivalently, additive in the density domain. There is substantial evidence to justify this for either photochemical or photo-electronic sensing and display systems. The discussion in Andrews and Hunt [21] is particularly illuminating in this regard. In general, however, the noise process $n(\underline{x})$ will depend upon the signal in a rather complicated fashion. We have chosen to disregard this dependence and assume a signal-independent noise process $n(\underline{x})$. Again this is common practice in digital image processing (cf. [21], pp. 20-23).

Taking the logarithm of both sides of (2) then results in the density image

$$g(\underline{x}) \triangleq \ln s_0(\underline{x}) = f_r(\underline{x}) + f_i(\underline{x}) + f_n(\underline{x}) \quad , \tag{3}$$

where $f_r(\underline{x}) \triangleq \ln r(\underline{x})$, $f_i(\underline{x}) = \ln i(\underline{x})$, and finally $f_n(\underline{x}) = \ln n(\underline{x})$. If precise stochastic descriptions of the signals $f_r(\underline{x})$, $f_i(\underline{x})$, and $f_n(\underline{x})$ are available the problem of sorting out the true image from the illumination and noise can

be formulated as one of Wiener or linear least mean-square filtering where the signal is $f_r(\underline{x})$ and the noise is $f_i(\underline{x})+f_n(\underline{x})$. Passing the result of this filtering through an exponentiation operation yields an estimate $\hat{f}(\underline{x})$ of the true image as represented by the reflectance process $r(\underline{x})$. A block diagram of the indicated processing is provided in Fig. 1.

The technique of sandwiching a linear operation between two complimentary nonlinear operations (homomorphic filtering) [7] as applied to image enhancement is not new; what is unique about the approach described here is the use of explicit stochastic image models as a guide in the choice of a linear filtering operation. In particular, we develop explicit stochastic models for both the reflectance process $f_r(\underline{x})$ and the illumination process $f_i(\underline{x})$. The reflectance process $f_r(\underline{x})$ has been developed to exhibit predominant and pronounced edge structure such as might be expected of real-world imagery. This process possesses considerable high spatial frequency components. The illumination process $f_i(\underline{x})$, on the other hand, has been specifically developed to possess relatively large low spatial frequency components typical of illumination fields. These stochastic models are described in Sections III and IV respectively. The noise process $f_n(\underline{x})$ is described in Section V while a description of the digital implementation of the Wiener filter is provided in Section VI. Some typical results are illustrated in Section VII which is followed by a summary and conclusions in Section VIII. We begin with some preliminary discussions on random fields as image models.

II. Preliminary Discussion:

The approach described earlier is not complete until the stochastic descriptions of $f_r(\underline{x})$, $f_i(\underline{x})$, and $f_n(\underline{x})$ are specified. The models to be considered

here will be a family of random variables $\{f_{\underline{x}}(\omega),\ \underline{x}\epsilon R^2\}$ defined on the plane where ω denotes the dependence on a fixed probability space (Ω,a,P). Wong [10] refers to such a collection as a <u>random field</u> but notes that it is also called a stochastic process with a several-dimensional time. In the discussion that follows, for convenience the dependence upon the underlying probability space will not be explicitly denoted; $f(\underline{x})$ will be written for $f_{\underline{x}}(\omega)$. Furthermore, consideration will be restricted to zero-mean fields of second order (variances exist). The second-order properties are described by the covariance function of the random field which is given by

$$R_{ff}(\underline{x},\underline{y}) = E\{f(\underline{x})f(\underline{y})\}\ ;\ \ \underline{x},\ \underline{y}\epsilon R^2\ , \tag{4}$$

where $E\{\cdot\}$ represents the expectation operator over the probability space (Ω,a,P). All of the random fields to be presented here have been constructed so as to possess a covariance function invariant under all Euclidean motions; according to the definitions of Wong [10] they are <u>homogeneous and isotropic</u>. For these fields (4) can be written

$$E\{f(\underline{x}+\underline{u})f(\underline{x})\}=R_{ff}(||\underline{u}||);\quad \underline{u}^T = (u_1,\ u_2)\epsilon R^2\ , \tag{5}$$

where $||\underline{u}||$ represents the Euclidean norm defined in terms of an inner product according to $||\underline{u}||^2= \langle\underline{u},\underline{u}\rangle = u_1^2 + u_2^2$. Since the random fields are homogeneous their power spectral density is given by

$$S_{ff}(\underline{\omega}) = \int_{R^2} R_{ff}(\underline{u})\exp\{-j\langle\underline{\omega},\underline{u}\rangle\}d\underline{u}\ , \tag{6}$$

where $\underline{\omega}^T = (\omega_1,\omega_2)$ represents a spatial frequency vector and $d\underline{u}$ is the differential volume element in R^2 . Furthermore, for isotropic fields $R_{ff}(\underline{u})=R_{ff}(||\underline{u}||)$ and (6) can be evaluated up to functional form with the aid of a theorem of Bochner [11] yielding

$$S_{ff}(\underline{\omega}) = S_{ff}(\Omega) = 2\pi \int_0^\infty \lambda R_{ff}(\lambda) J_0(\lambda\Omega) d\lambda \quad , \tag{7}$$

where $\Omega \triangleq ||\underline{\omega}|| = (\omega_1^2+\omega_2^2)^{1/2}$ represents radial frequency and $J_0(\cdot)$ denotes the ordinary Bessel function of the first kind of order zero. Thus $S_{ff}(\cdot)$ and $R_{ff}(\cdot)$ are related through a Hankel transform [12], [13].

The enhancement problem as we have posed it consists of emphasizing $f_r(\underline{x})$ while minimizing the degrading effects of $f_i(\underline{x}) + f_n(\underline{x})$; specifically we will look for the linear least mean-squared estimate of $f_r(\underline{x})$ based on observing $g(\underline{x})$. If we have knowledge of the power spectral densities† $S_{rr}(\underline{\omega})$, $S_{ii}(\underline{\omega})$, and $S_{nn}(\underline{\omega})$ associated with $f_r(\underline{x})$, $f_i(\underline{x})$, and $f_n(\underline{x})$ respectively, and these three fields are uncorrelated, the 2-dimensional (2-D) linear least mean-square filter possesses transfer function

$$H_0(\underline{\omega}) = \frac{S_{rr}(\underline{\omega})}{S_{rr}(\underline{\omega})+S_{ii}(\underline{\omega})+S_{nn}(\underline{\omega})} \quad , \tag{8}$$

which is simply an extension to 2-dimensions of the Wiener filter [5].

We will now proceed to describe the random fields which are to be used as the reflectance, illuminance, and noise models respectively.

III. Reflectance Process:

The process to be considered as a model of the reflectance will be referred to as the "rectangular process". This process divides the plane into regions whose boundaries form rectangles and then assigns intensities to these regions such that the intensity within each region is constant and possesses specified correlation properties with intensities in contiguous regions. It was originally developed to satisfy the need for an edge model for the design of a linear filter-

† In general, the power spectral density of a random field $f(\underline{x})$ will be denoted by $S_{ff}(\underline{\omega})$. In situations where subscripts are used, such as $f_r(\underline{x})$, the corresponding power spectral density will be distinguished by the associated subscript, i.e., $S_{rr}(\underline{\omega})$ in the case of $f_r(\underline{x})$.

ing operation to be used in edge detection [15]. Roughly speaking it is a 2-D extension of a generalization of the random telegraph wave [14].

As a first step in describing this process, the method of partioning the plane into rectangles will be detailed. A fundamental role in this stochastic image model will be played by the vector valued random field $\underline{N}(\underline{x})$ which provides a two-dimensional generalization of a counting process. In particular, suppose the vector $\tilde{\underline{x}}$ is obtained from $\underline{x}$ according to $\tilde{\underline{x}} = \underline{\underline{A}}\underline{x}$ where $\underline{\underline{A}}$ is the matrix

$$\underline{\underline{A}} = \begin{bmatrix} \cos\theta & \sin\theta \\ -\sin\theta & \cos\theta \end{bmatrix} , \tag{9}$$

defined for some $\theta\varepsilon[-\pi,\pi]$. The transformation (9) then results in a rotation of the plane in terms of the Cartesian coordinate axis (x_1,x_2) as illustrated in Fig. 2. Consider now the vector-valued random field defined by

$$\underline{N}(\underline{x}) = (N_1(\tilde{x}_1) , N_2(\tilde{x}_2)) , \tag{10}$$

where θ is uniformly distributed on $[-\pi,\pi]$ and $\{N_i(t), t \geq 0\}$, i=1,2 are mutually independent one-dimensional counting processes, i.e., $N_i(t)$ represents the number of events which have occurred in the interval $[0,t]$. Specifically, let the probability density function p(t) of the distance between events) be given by the exponential distribution function

$$p(t) = \lambda_r e^{-\lambda_r t}; \; t \geq 0 . \tag{11}$$

The quantity λ_r represents the average number of events per unit distance.

Consider now the random field $\{f_r(\underline{x}), \underline{x}\varepsilon R^2\}$ which undergoes transitions at the boundaries of the elementary rectangles defined by $\{\underline{N}(\underline{x}), \underline{x}\varepsilon R^2\}$. The gray level assumed throughout any elementary rectangle will be assigned

so as to be zero-mean Gaussian† with variance σ_r^2 and correlated with the gray levels in contiguous rectangles. More specifically, assume that the random orientation $\theta\varepsilon[-\pi,\pi]$ has been chosen and that k transitions have occurred between the two points $\underline{x}$ and $\underline{x}+\underline{u}$. It will be assumed that

$$E\{f(\underline{x}+\underline{u})f(\underline{x})|\theta,k\} = \sigma_r^2\rho_r^k; \quad k=0,1,\ldots, \tag{12}$$

where $|\rho_r|\leq 1$. The quantity ρ_r is the correlation coefficient governing the spatial evolution of the random amplitude process. For example, let $X_{i,j}$ represent the amplitude or gray level assigned after i transitions in the $\tilde{x}_1$ direction and j transitions in the $\tilde{x}_2$ direction. The sequence $\{X_{i,j}\}$ can then be generated recursively according to

$$X_{i,j} = \rho_r X_{i-1,j} + \rho_r X_{i,j-1} - \rho_r^2 X_{i-1,j-1} + W_{i,j} \quad , \tag{13}$$

where $\{W_{i,j}\}$ is a 2-D sequence of independent and identically distributed (i.i.d.) zero mean Gaussian variates with common variance $\sigma_w^2=\sigma_r^2(1-\rho_r^2)^2$. The sequence defined by (13) has an alternative interpretation as the output of a recursive 2-D digital filter excited by a white noise field.

It can be shown that

$$E\{X_{i,j}X_{i+k_1,j+k_2}\} = \sigma_r^2\rho_r^{|k_1|+|k_2|} \quad , \tag{14}$$

so that the condition expressed by (12) is indeed satisfied.

Typical computer-generated realizations of the resulting random field are illustrated in Fig. 3 for selected values of ρ_r and λ_r. Note that λ_r controls the edge density while ρ_r indicates the degree of correlation of intensities in adjacent regions. The displayed images here and throughout the remainder of this paper are square arrays consisting of 256 elements or samples on a side. Where a value of λ_r is specified it is measured in normalized units of

---

† The Gaussian assumption here is not critical and is easily removed.

events per sample distance so that there are on average $256\lambda_r$ transitions along each of the orthogonal axes.

In [15] it has been shown that the power spectral density of this process is given by

$$S_{rr}(\Omega) = \frac{8(1-\rho_r)\lambda_r\sigma_r^2}{\Omega^2+2(1-\rho_r)^2\lambda_r^2}\left[\frac{1}{\Omega^2+(1-\rho_r)^2\lambda_r^2}\right]^{1/2} . \qquad (15)$$

Although realizations of this process may not resemble any particular real-world image, the general properties of regions of constant reflectivity and boundaries of regions being parallel are common to many real-world images. More specifically, we do not claim that the model proposed here is universally representative of real-world imagery except in a certain qualitative sense. This model is completely defined, up to a scale factor, by the two parameters λ_r and ρ_r. The parameter λ_r represents the "edge busyness" associated with an image while ρ_r is indicative of the degree of abruptness across an edge boundary. For ρ_r large (in magnitude) and negative there is an abrupt almost black-to-white or white-to-black transition across an edge boundary. For $\rho>0$, on the other hand, the transition across an edge boundary is much more gradual. These properties are easily related to any particular real-world image.

IV. Illumination Process:

In the previous section a 2-D random field which possesses an inherent rectangular structure was described and analyzed. While this random field is a reasonable model of objects, shadows do not generally exhibit this rectangular mosaic but rather a much more random edge orientation. Here the construction and properties of a class of 2-D random fields which provide a more appropriate model for illumination in the sense that individual realizations do not exhibit this rectangular pattern will be presented. Consider the random

partition of the plane by a series of sensed (directed) lines which can be described as a marked point process. Specifically, an arbitrary sensed line can be described in terms of a 3-tuple (r,θ,d) where r represents the perpendicular distance or radius to the line in question, $\theta\varepsilon[-\pi,\pi]$ represents the orientation of the vector of length r drawn from the origin and perpendicular to this line, and $d\varepsilon\{-1, 1\}$ specifies the sense of the line where Fig. 4 illustrates a case of d=1 (pointing counterclockwise). As shown in Fig. 4, by virtue of the direction imposed on this line segment the plane is partitioned into two distinct regions, R(right of line) and L(left of line) such that $R \cup L=R^2$.

Now consider the set of lines represented by the sequence $\{(r_i,\theta_i,d_i)\}$. Here $\{r_i\}$ represents the event positions associated with a homogeneous Poisson process $\{N(r),r \geq 0\}$ with intensity λ events/unit distance evolving according to the radial parameter r. The sequence $\{\theta_i\}$ represents an (i.i.d.) sequence of random variables uniformly distributed on $[-\pi,\pi]$ while the sequence $\{d_i\}$ is likewise i.i.d. assuming the binary values ± 1 with equal probability. Finally, the sequences $\{r_i\}$, $\{\theta_i\}$ and $\{d_i\}$ are assumed to be independent.

Now note that the set of lines generated by the process described above will divide the plane into disjoint polygonal regions. For any point $\underline{x}$ define $N_{LR}(\underline{x})$ to be the number of left-to-right crossings of sensed lines incurred in moving along a straight path from the origin to the point $\underline{x}$; similarly define $N_{RL}(\underline{x})$ to be the number of right-to-left crossings. Observe that $N_{LR}(\underline{x}_1) = N_{LR}(\underline{x}_2)$ and $N_{RL}(\underline{x}_1) = N_{RL}(\underline{x}_2)$ for any two points $\underline{x}_1$ and $\underline{x}_2$ which are in the same region. Assign a label k to each region as $k = N_{LR}(\underline{x}) - N_{RL}(\underline{x})$ where $\underline{x}$ is a point in the region. This label can in turn be used to assign a gray level to each region by using it to index into a sequence $\{X_k\}$ of zero-mean Gaussian random variables. In particular, assume that the

sequence $\{X_k\}$ is generated recursively according to

$$X_k = \rho_i X_{k-1} + W_k \qquad ; k = 1,2,\ldots ,$$

and (16)

$$X_k = \rho_i X_{k+1} + W_k \qquad ; k = -1,-2,\ldots ,$$

with $\{W_k\}$ an i.i.d. zero mean Gaussian sequence with variance $\sigma_w^2 = (1-\rho_i^2)\sigma_i^2$ and the initial value X_0 chosen to have zero-mean Gaussian distribution with variance σ_i^2. Note that this sequence is stationary with covariance given by

$$E\{X_k X_{k+n}\} = \sigma_i^2 \rho_i^{|n|} . \tag{17}$$

Selected computer-generated realizations of the resulting random field are illustrated in Fig. 5 for various values of ρ_i and $\lambda_i \triangleq \lambda/\pi$. The quantity λ_i can be shown to represent the average edge density along any randomly chosen line segment on the plane. From Fig. 5 observe that for $\rho = 0.5$ light regions tend to be surrounded by light regions while for $\rho_i = -0.9$ there is a tendency for light regions to be surrounded by dark regions and vice versa. Indeed, in the latter case there is almost a black-to-white or white-to-black inversion across an edge boundary.

An expression for the autocorrelation function given by (4) can be obtained as in [17] with the result

$$R_{ii}(\underline{u}) = \sigma_i^2 e^{-\lambda_i ||\underline{u}||} \{I_0(\lambda_i ||\underline{u}||) + 2 \sum_{k=1}^{\infty} \rho_i^k I_k(\lambda_i ||\underline{u}||)\} , \tag{18}$$

where $I_k(\cdot)$ is the modified Bessel function of the first kind of order k. Similarly, the corresponding power spectral density evaluated according to (7) is given by

$$S_{ii}(\Omega) = \frac{2\sigma_i^2(1-\rho_i^2)}{\lambda_i^2} \int_0^{\pi} \left[\frac{1-\cos\phi}{1-2\rho_i\cos\phi+\rho_i^2}\right] \frac{d\phi}{[(\Omega/\lambda_i)^2+(1-\cos\phi)^2]^{3/2}} , \tag{19}$$

which is illustrated in Fig. 6 for various values of ρ_i. One noteable characteristic of this random field is that for Ω small compared to λ_i, the power spectral density behaves approximately as $\Omega^{-3/2}$, i.e., $S_{ii}(\Omega)$ has a singularity at the origin except for $\rho_i = -1$. This high concentration of energy at low spatial frequencies is a direct result of the construction procedure which allows relatively large correlation between gray levels in regions relatively far apart. We feel that this characteristic is typical of random illumination processes and as a result it was purposely built into the construction procedure.

The effect on a real-world image of multiplying the intensity by the exponential of a realization of the polygonal process is illustrated in Fig. 7. Note how the illumination process seems simply to have added extra shadows to the building. Although somewhat of an exageration, this figure has been included to illustrate the nature of effects which may be caused by the proposed random illumination process.

V. White Noise Process:

In any image that is scanned there is some noise present that is independent from pixel-to-pixel; due to its appearance it is often referred to as "salt-and-pepper noise". Here we will model this noise, which is represented by $f_n(\underline{x})$, as white Gaussian noise. While the Gaussian assumption is not critical to the analysis which follows it is interesting to note the observation of Selwyn (cf. [2], pg. 125) on noise due to film grains. He notes that if the spot area covered by a beam used to measure the density of a photographic emulsion is much larger than the projection of individual grains then the density distribution will be Gaussian if the grain noise is small, and presumably homogeneous. In fact, the following relationship between the size of the scanning aperture and variance of the measured densities has been found to hold:

$$\sigma_n^2 = G^2/2a \ , \tag{20}$$

where σ_n^2 is the variance of the density, G is a measure of the granularity of the film, and a is the area of the scanning aperture. If the scanning aperture is considered to be a spatial lowpass filter whose bandwidth is proportional to $1/\sqrt{a}$ then (20) implies that the noise power present in the density measurement is proportional to the lowpass filter bandwidth squared. Since this is the effect that would be observed if the grain noise were white this modeling assumption is justified. The power spectral density of this noise can be expressed then as

$$S_{nn}(\Omega) = \sigma_n^2 \ , \tag{21}$$

where σ_n^2 is the variance of the samples.

VI. Linear Filter Description and Implementation:

Using the models presented above the linear least mean-squared error (Wiener) filter for estimating the reflectance process will now be derived. The system transfer function given by (8) can be rewritten as

$$H_0(\underline{\omega}) = \frac{1}{1 + \dfrac{S_{ii}(\underline{\omega})}{S_{rr}(\underline{\omega})} + \dfrac{S_{nn}(\underline{\omega})}{S_{rr}(\underline{\omega})}} \ , \tag{22}$$

which suggests defining the parameters γ_i and γ_n as the ratios of illumination and noise powers to reflectance power respectively. These parameters provide a measure of the degree of degradation caused by shadows and salt-and-pepper noise. More specifically, we have

$$\gamma_i \triangleq \sigma_i^2/\sigma_r^2 \tag{23}$$

while

$$\gamma_n \triangleq \sigma_n^2/\sigma_r^2 \tag{24}$$

so that the filter is completely specified in terms of the quantities γ_i, γ_n, ρ_r, λ_r, ρ_i, and λ_i. Finally, observe that for the given power spectral densities the filter is radially symmetric, i.e., it is a function of $\Omega = ||\underline{\omega}||$.

Since the final objective of this process is to make the best use of the limited dynamic range available for display it will prove expedient to include a gain factor A_0 chosen such that the power leaving the linear processor equals that entering. It follows then that A_0 is given by

$$A_0 = \sqrt{\iint S_{gg}(\underline{\omega})d\underline{\omega} / \iint |H_0(\underline{\omega})|^2 S_{gg}(\underline{\omega})\, d\underline{\omega}} \quad , \tag{25}$$

where $S_{gg}(\underline{\omega})$ is the power spectral density of the filter input $g(\underline{x})$ in (2) and is given by

$$S_{gg}(\underline{\omega}) = S_{rr}(\underline{\omega}) + S_{ii}(\underline{\omega}) + S_{nn}(\underline{\omega}) \ . \tag{26}$$

The description of the filter provided above is for a continuous spatial domain; we have access only to sampled data. Hence we seek a (2-D) digital filter with system transfer function $H_0(z_1, z_2)$ whose frequency response† approximates $H_0(\Omega)$. Specifically, the Wiener filter has been implemented as a 2-D infinite impulse response (IIR) [18] digital filter whose point spread function exhibits quadrant symmetry. The choice of an IIR filter was based on the computational economies which result from the ability to implement the filter with a recursive structure. Consider first a filter with the following recursive structure:

$$y_{m,n} = - \sum_{(i,j)\in D'} a_{i,j}\, y_{m-i,n-j} + \sum_{(i,j)\in D} b_{i,j}\, x_{m-i,n-j} \tag{27}$$

---

† The frequency response of the two-dimensional digital filter is simply $H_0(z_1, z_2)$ evaluated for $z_i = e^{j\omega_i}$, i=1,2. We assume the spatial frequency variable ω_i is measured in units of radians per sample distance.

where[†] $D \triangleq \{(i,j):\ i=0,1,\ldots,N\ ,\ j=0,1,\ldots,M\}$ and $D' = D - \{(0,0)\}$. At this point we will assume that the coefficients of y in (32) have been chosen such that the resulting filter is stable when recursing from the upper left-hand corner. Observe that the resulting filter will have nonzero response only in the lower right quadrant. Since the filter described in (22) exhibits radial symmetry it is desirable for the resulting digital filter to exhibit four-quadrant symmetry.

One method for achieving a point spread function with this inherent symmetry is to allow repeated application of the same filter recursing from each of the four corners. If $\{h_{i,j}\}$ represents the point spread function associated with a single application of the filter specified by (27) then the composite filter possesses point spread function as indicated in Fig. 8. The corresponding system transfer function of the composite filter is then

$$H(z_1,z_2) = H_0(z_1,z_2)+H_0(z_1^{-1},z_2)+H_0(z_1,z_2^{-1})+H_0(z_1^{-1},z_2^{-1}), \tag{28}$$

where $H_0(z_1,z_2)$ is the transfer function corresponding to (27) and is given by

$$H_0(z_1,z_2) = \sum_{(i,j)\in D} b_{i,j}z_1^{-i}z_2^{-j} \Big/ \left[1+\sum_{(i,j)\in D'} a_{i,j}z_1^{-i}z_2^{-j}\right] \tag{29}$$

In choosing $H_0(z_1,z_2)$ to provide an approximation to $H_0(\Omega)$ for $z_i=e^{j\omega_i}$, i=1,2 we have restricted attention to the case where $H_0(z_1,z_2)$ is a second order section of the form

$$H_0(z_1,z_2) = \frac{b_{00}+b_{01}(z_1^{-1}+z_2^{-1})+b_{11}(z_1^{-1}z_2^{-1})+b_{02}(z_1^{-2}+z_2^{-2})}{1+a_{01}(z_1^{-1}+z_2^{-1})+a_{11}(z_1^{-1}z_2^{-1})+a_{02}(z_1^{-2}+z_2^{-2})} \tag{30}$$

with the restriction

$$b_{00} = -2b_{01} - b_{11} - 2b_{02} \tag{31}$$

This choice insures zero frequency response at the origin and symmetry of the

---

[†] The support D of the recursive 2-D filters taken here will be such as to force a quarter plane causality condition. That is, D consists of a finite number of points above and to the left of the pixel in position (i,j).

corresponding point spread function about a line 45° to the axis; i.e., $h_{i,j}=h_{j,i}$. Similar properties extend, of course, to the composite filter represented by $H(z_1,z_2)$. A computer program has been written for determining the coefficients b_{00}, b_{01}, b_{11}, b_{02}, a_{01}, a_{11} and a_{02} according to an iterative gradient procedure to result in a frequency response for $H(z_1,z_2)$ which provides a least mean-squared error approximation to the desired response $H_0(\Omega)$. The details of this program are described in [6]. In Table 1 we summarize the results of this procedure for selected values of γ_i, λ_i, ρ_i, λ_r, and ρ_r, all with γ_n=-20dB. Here we have found it convenient to classify the shadow characteristic as soft, medium or harsh depending upon the value of γ_i.

Shadow Characteristic	γ_i(dB)	λ_i	ρ_i	λ_r	ρ_r	a_{01}	a_{11}	a_{02}	b_{00}	b_{01}	b_{11}	b_{02}
Soft	-6	.0125	0.5	.05	0	-.8650	.7830	-.0240	.2376	-.1957	.1831	-.0147
Medium	-3	.0125	0.5	.05	0	-.8503	.7743	-.0326	.2681	-.2216	.2072	-.0160
Harsh	6	.0125	-.9	.05	0	-.8817	.7959	-.0118	.5109	-.4718	.4458	-.0065

Table 1

Typical Filter Parameters for γ_n=-20dB

For the three cases described in Table 1, the corresponding power spectral densities $S_{rr}(\Omega)$ and $S_{ii}(\Omega)$ together with the resulting Wiener filter response $H_0(\Omega)$ are plotted in Fig. 9 as a function of the radial frequency variable Ω. Observe the sharp DC rejection in all cases. This is, of course, due to the relatively high concentration of energy at low spatial frequencies associated with the illumination process $f_i(\underline{x})$ as described previously. The Wiener filter response $H_0(\Omega)$ exhibits the essential characteristics of the linear highpass

filter originally proposed by Stockham [4] on an ad hoc basis. It is of some interest that this choice can be justified rigorously under the modeling assumptions made here.

In Fig. 10 we illustrate 3-dimensional plots of one quarter-plane of the frequency response of the filters associated with the three cases described in Table 1. The left hand column shows the desired responses while the right hand column illustrates the responses obtained by the digital filters. The frequencies displayed run from 0 at the front to π radians per pixel at the back. Note that in all cases the complete attenuation of DC and rolloff at higher frequencies have been preserved in the transition from the desired analog filters to the digital approximations.

VII. Results:

The algorithm presented above has been applied to several real world images for selected values of the parameters γ_n, γ_i, ρ_r, λ_r, ρ_i, and λ_i. The processed images shown here illustrate the effects of varying these parameters on the reconstructed images.

Parts a of each of the four sets of images composing Fig.'s 11 through 14 are the original images while parts b, c, and d are the corresponding processed versions. All of the processed images have the salt-and-pepper noise 20 dB below the reflectance and the reflectance has zero correlation of intensities in different regions (ρ_r=0) and an edge density such that on the average there will be 12 transitions on a side of the image (λ_r=.05). The variations among b, c, and d are due to changes in the illumination intensity γ_i, and the illumination correlation ρ_i.

Part b of these figures has the edge density of the illumination process λ_i = .0125 or, on the average, 3 transitions on a side of the image, ρ_i=0.5 (positive correlation of illumination in adjacent regions) and illumination power 6 dB below reflectance power (γ_i=-6 dB), corresponding to a soft shadow.

Note how in part b local variations are much more evident; shadow and highlight detail have both been emphasized. Specifically, in Fig. 11b detail in the hair is much more evident than in 11a. In Fig. 12b the light scaffolding blends in less with the clouds while the dark slatting on the side of the tower is also more evident. Similarly, in Fig. 13b the bright regions in the center have been de-emphasized and detail in the building is more apparent. Finally, for the forward looking infrared (FLIR) image in Fig. 14b the tank blends in less with its surroundings. This processing brings out detail in both dark and light areas.

Parts c (medium shadow) of Fig.'s 11-14 vary from parts 'b in the increase of the illumination power by 3dB. The effects noted above have simply become more evident.

Part d (harsh shadow) deviates from c in both illumination power (which is increased by 9dB) and the correlation of illuminances in different regions which is now -0.9 instead of 0.5. Part d of all the figures brings out detail in adjacent light and dark regions better than c as is expected from the shadow being modeled as having balck-to-white transitions across boundaries between adjacent regions.

An application of this technique to a dynamic range reduction problem is illustrated in Fig. 15. In the original tomograph image, little detail is evident in the dark area while the light areas appear muddy. In Fig. 15b some detail is evident in the dark region while local shading is more apparent in light regions. When harsher shadows are assumed, as in 15c and 15d, local detail is amphasized.

In all cases the processing has increased the visibility of detail in such a way that less scrutiny need be applied when observing the processed images than is required when observing the originals. There are, however, differences in the characteristics of the processing that occurs. Increasing the shadow power and making the shadow more pronounced by having negative correlation (ρ=-0.9) instead of positive correlation (ρ=0.5) has made local detail more visible by suppressing variations in intensity that occur over large regions.

VIII Summary and Conclusions:

A method for determining the linear filtering operation to be performed as part of homomorphic processing based on Wiener filtering concepts has been described. The resulting linear filter is determined by the parameters of the assumed stochastic models of the signal and degradation. These parameters are associated with salient characteristics of the signal and degradation. Although no claims can be made about the optimality of a particular filter for any given real-world image it has been shown that the parameters in the models provide a useful means for specifying the desired effects of the processing.

The implementation of the linear operation has taken the form of a 2-D recursive IIR digital filter whose order has been restricted to result in computational efficiency and whose coefficients have been chosen to result in a good approximation to the Wiener filter.

The resulting nonlinear filtering operation has been applied to a number of real-world images to illustrate the relationship between the parameters of the assumed stochastic models and the effects of the resulting processing.

References

1. W.D., Zoethout , Physiological Optics, The Professional Press, Chicago, Ill. pp. 157, 1939.

2. P. Kowaliski , Applied Photographic Theory, Wiley, New York, 1972.

3. J. E. Hochberg , Perception, Prentice-Hall, Englewood Cliffs, N.J., 1964.

4. T. G. Stockham , "Image Processing in the Context of a Visual Model", Proceedings of the IEEE, Vol. 60, No. 7, pp 828-842, July 1972.

5. H. L. Van Trees , Detection, Estimation and Modulation Theory;Vol. 1, Wiley,N.Y.1968.

6. R. W. Fries , "Theory and Application of a Class of Two-Dimensional Random Fields", Ph.D. Thesis, RPI, Troy, N.Y., in preparation.

7. A. V. Oppenheim, R. W. Schafer ,and T.G. Stockham, Jr., "Nonlinear Filtering of Multiplied and Convolved Signals", Proc. IEEE, Vol. 56, pp 1264-1291, Aug. 1968.

8. E. Wong , "Homogeneous Gauss-Markov Random Fields", Ann. Math. Stat.,Vol. 40, pp. 1625-1634, 1969.

9. E. Wong , "Two-Dimensional Random Fields and the Representation of Images", SIAM J. Appl. Math.,Vol. 16, pp. 756-770, 1968.

10. E. Wong , Stochastic Processes in Information and Dynamical Systems, Chap 7, McGraw-Hill, New York, 1971.

11. S. Bochner , Lectures on Fourier Integrals, Annals. of Math. Studies, No. 42, Princeton Univ. Press, Princeton, N.J., pp.235-238, 1959.

12. A. Papoulis , "Optical Systems, Singularity Functions, Complex Hankel Transforms", J. Opt. Soc. Amer., Vol. 57, pp. 207-213, 1967.

13. A. Papoulis , Systems and Transforms with Applications in Optics, McGraw-Hill, New York, 1968.

14. J. W. Modestino and R. W. Fries , "A Generalization of the Random Telegraph Wave", submitted to IEEE Trans. on Inform. Theory.

15. J. W. Modestino and R. W. Fries , "Edge Detection in Noisy Images Using Recursive Digital Filtering", Computer Graphics and Image Processing,6, pp. 409-433, Oct. 1977.

16. J. W. Modestino , R. W. Fries and D. G. Daut , "A Generalization of the Two-Dimensional Random Checkerboard Process",to appear in J. Opt. Soc. Amer.

17. J. W. Modestino and R. W. Fries , "Construction and Properties of a Useful Two-Dimensional Random Field", submitted to IEEE Trans. on Inform.Theory.

18. L. R. Rabiner and B. Gold, Theory and Applications of Digital Signal Processing, Prentice-Hall, Englewood Cliffs, N.J.,pg.451, 1975.

19. C. Shipman, Understanding Photography, H. P. Books, Tucson, Arizona, 1974.

20. J. Mannos and D. L. Sakrison,"The Effects of a Visual Fidelity Criterion on the Encoding of Images", IEEE Trans. Inform. Theory, Vol. 20, pp. 525-536, 1974.

21. H. C. Andrews and B. R. Hunt, Digital Image Restoration, Prentice-Hall, Englewood Cliffs, NJ, 1977.

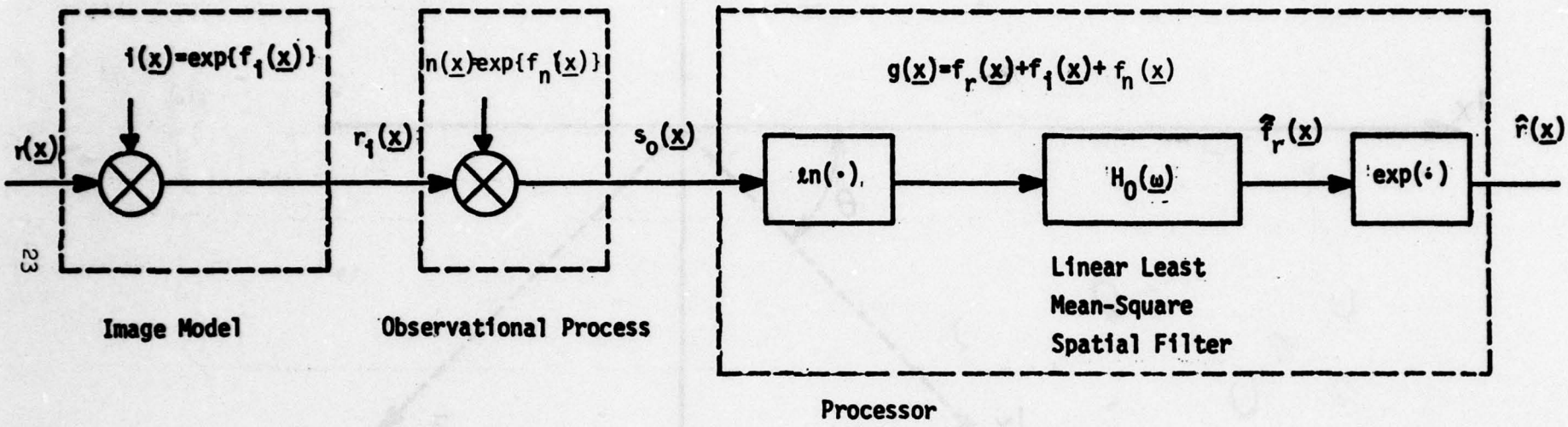

Figure 1

Homomorphic Filtering of Degraded Imagery

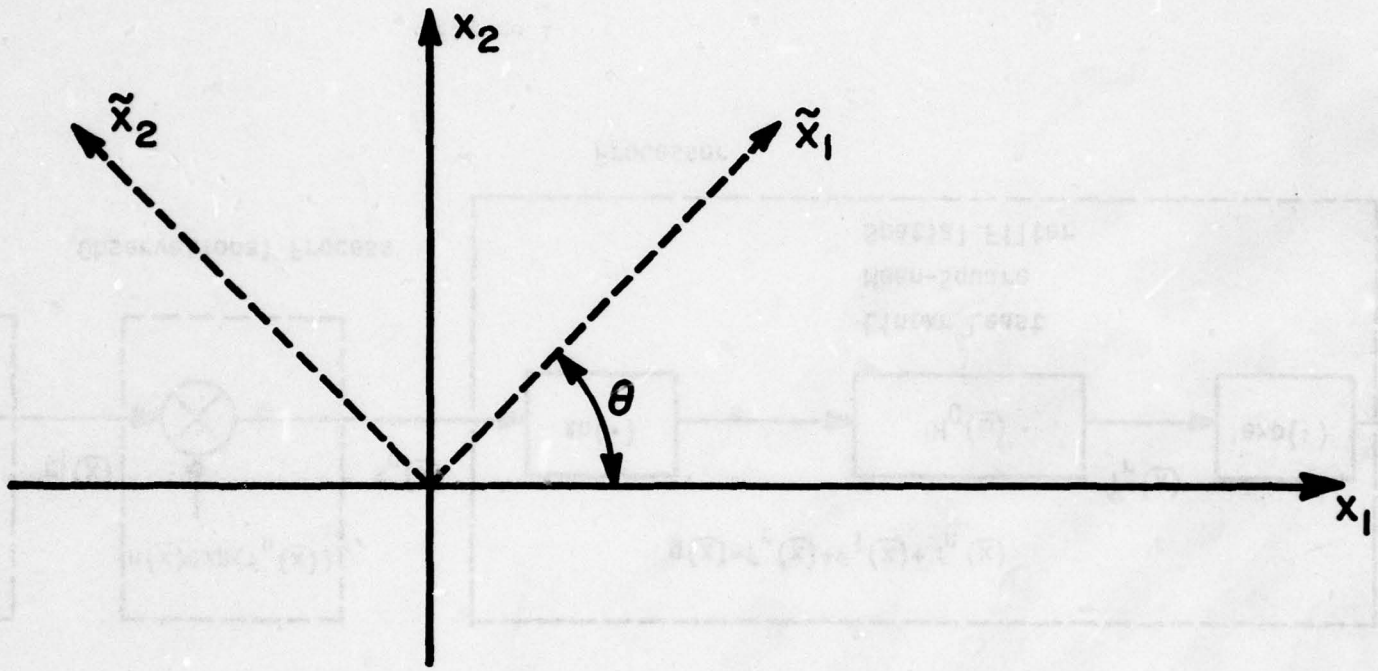

Figure 2

Rotation of Cartesian Coordinate Axes

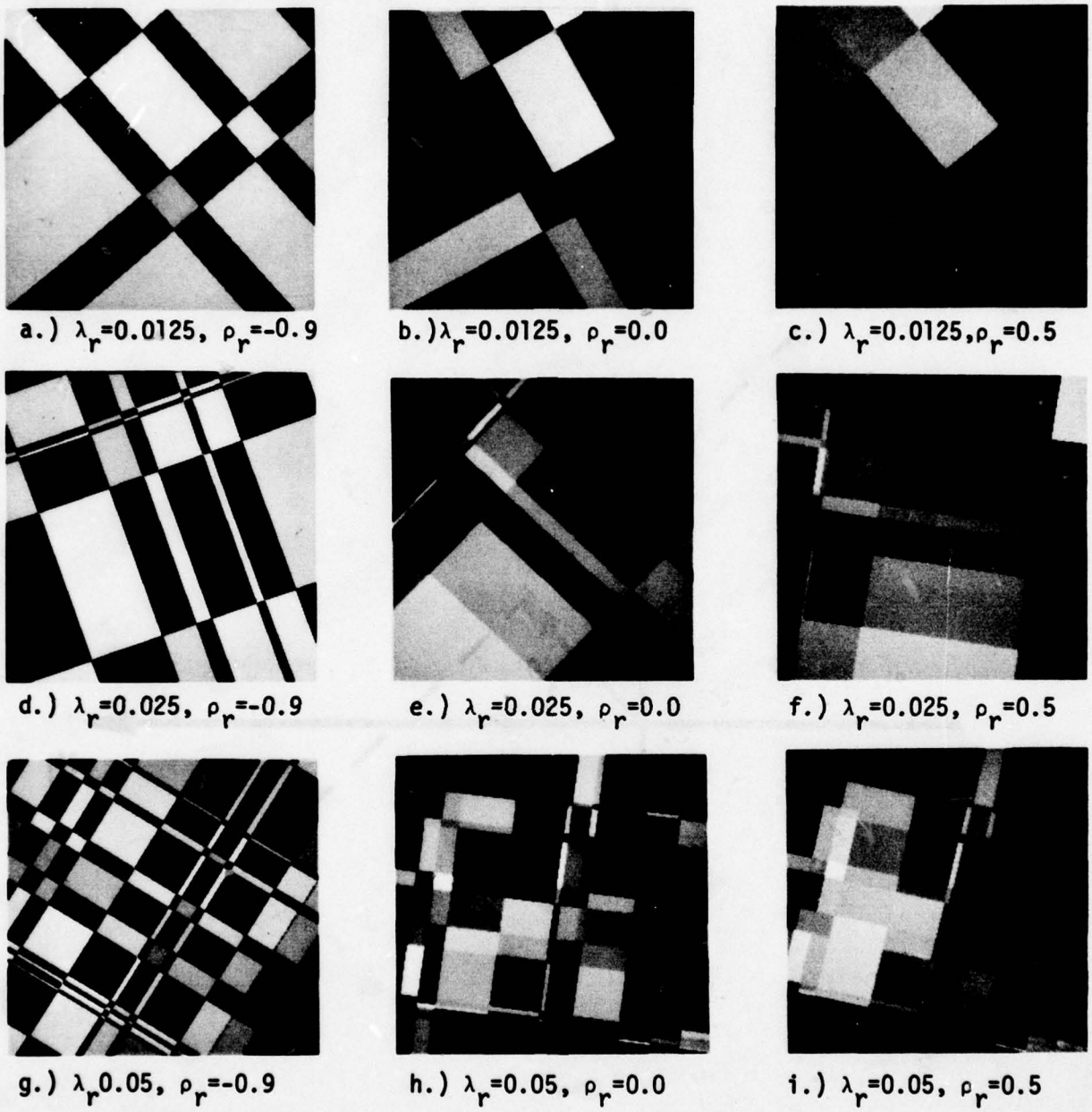

a.) λ_r=0.0125, ρ_r=-0.9 b.)λ_r=0.0125, ρ_r=0.0 c.) λ_r=0.0125,ρ_r=0.5

d.) λ_r=0.025, ρ_r=-0.9 e.) λ_r=0.025, ρ_r=0.0 f.) λ_r=0.025, ρ_r=0.5

g.) λ_r0.05, ρ_r=-0.9 h.) λ_r=0.05, ρ_r=0.0 i.) λ_r=0.05, ρ_r=0.5

Figure 3

Selected Realizations of Reflectance Process

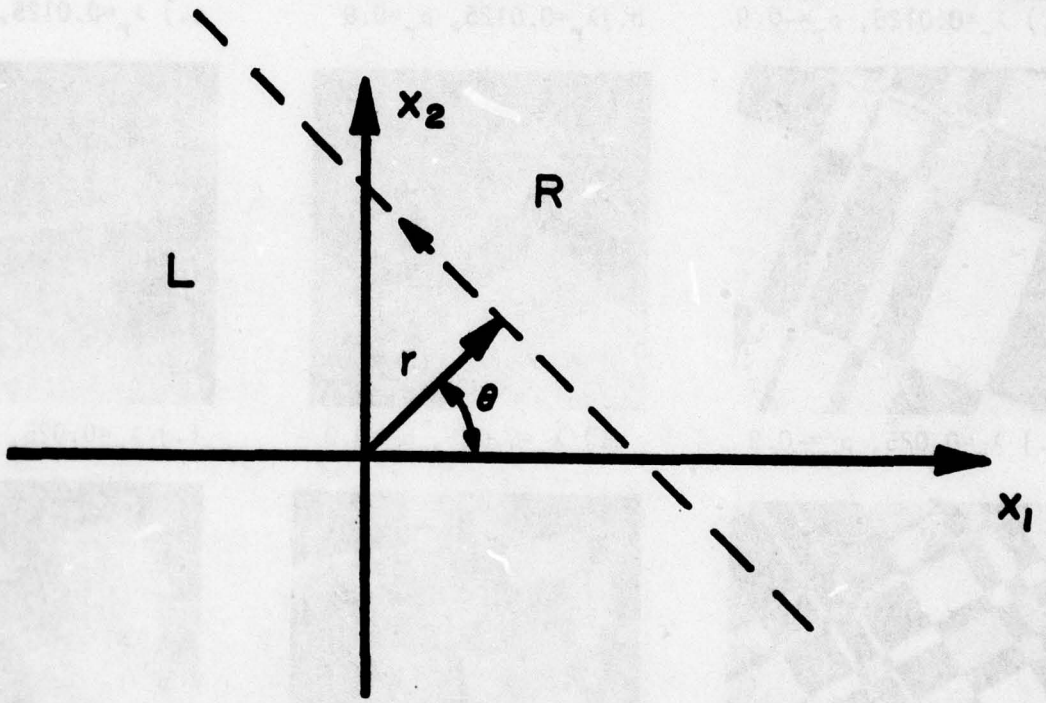

Figure 4

Parameterization of Directed Line Segment

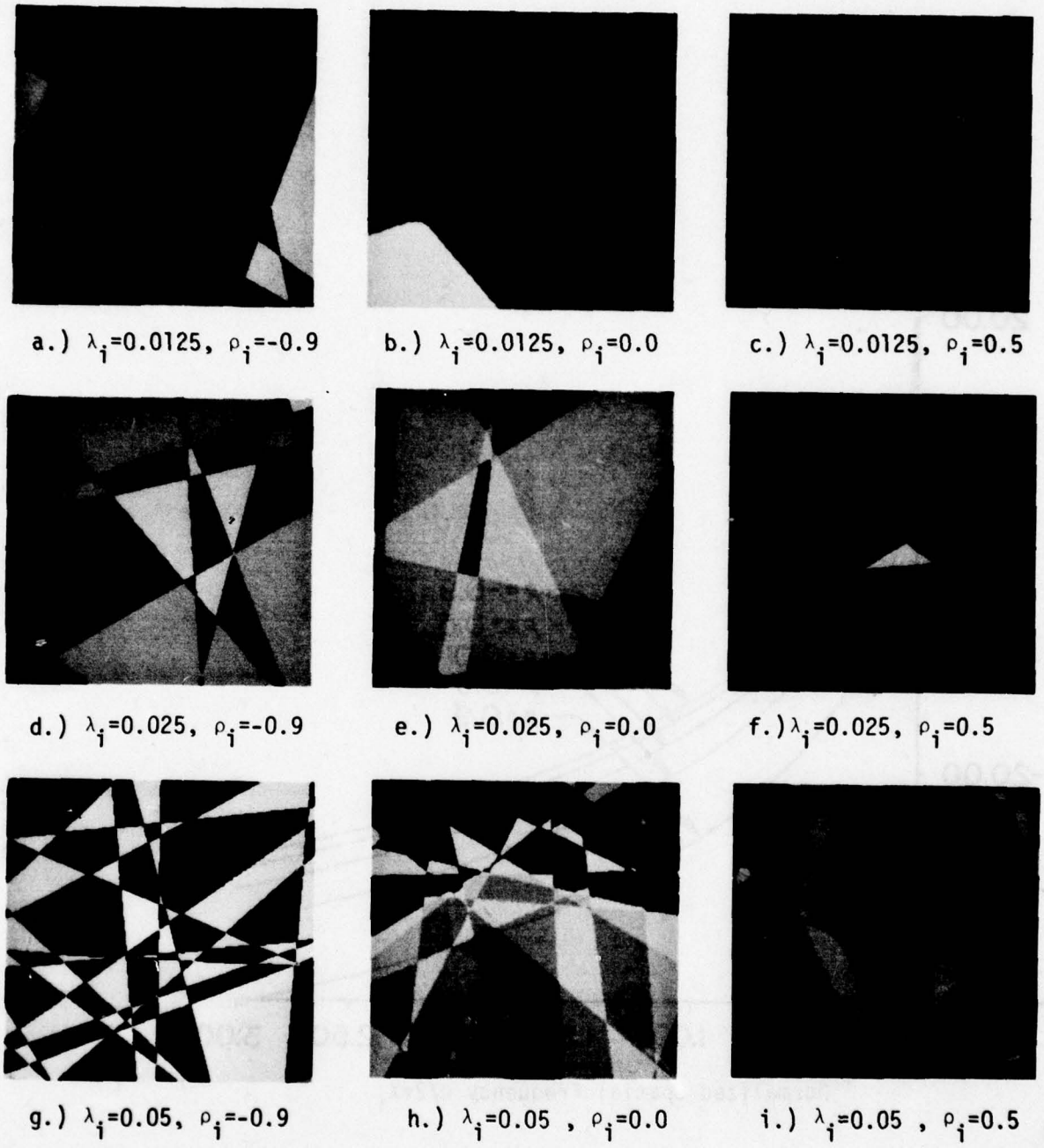

a.) λ_i=0.0125, ρ_i=-0.9 b.) λ_i=0.0125, ρ_i=0.0 c.) λ_i=0.0125, ρ_i=0.5

d.) λ_i=0.025, ρ_i=-0.9 e.) λ_i=0.025, ρ_i=0.0 f.) λ_i=0.025, ρ_i=0.5

g.) λ_i=0.05, ρ_i=-0.9 h.) λ_i=0.05 , ρ_i=0.0 i.) λ_i=0.05 , ρ_i=0.5

Figure 5
Selected Realizations of Illumination Process

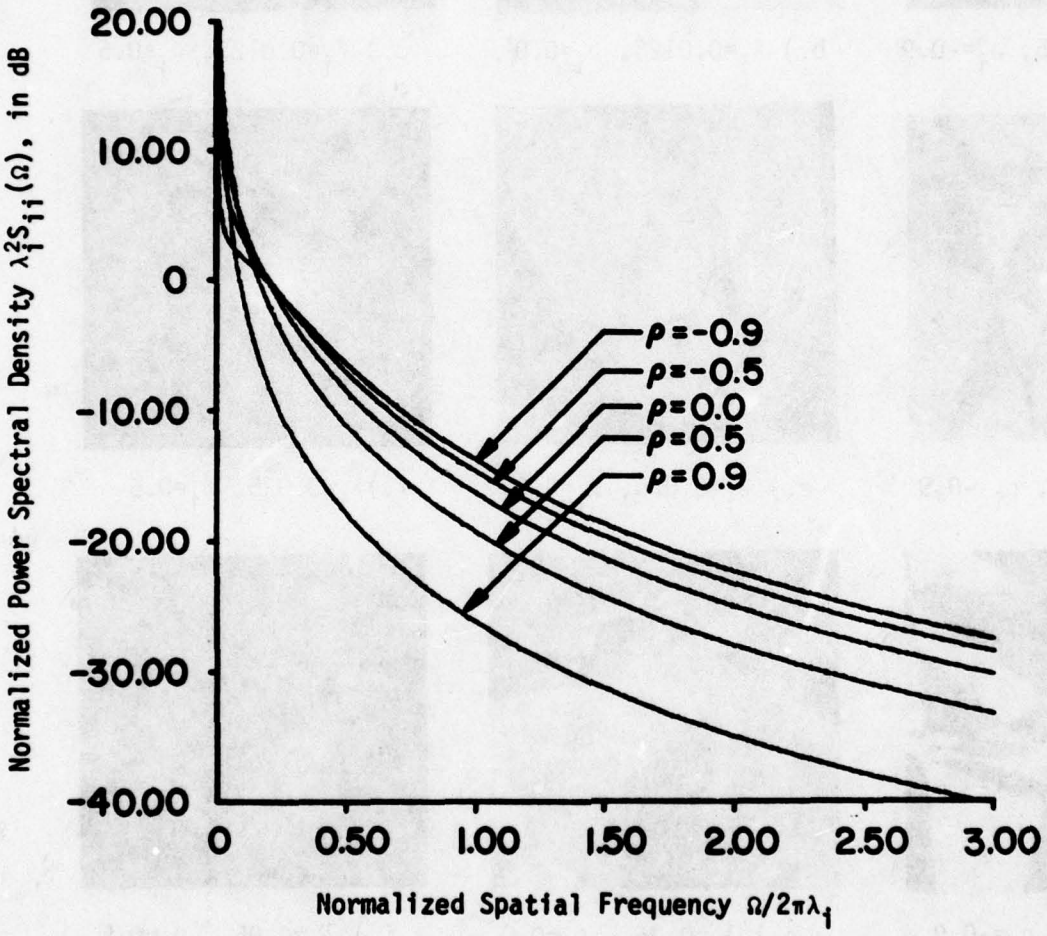

Figure 6

Power Spectral Density of Illumination Process

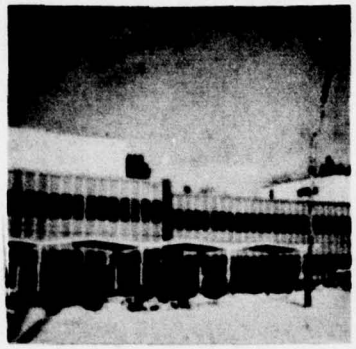

a.) Original

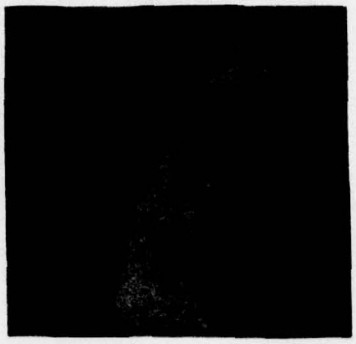

b.) Illumination

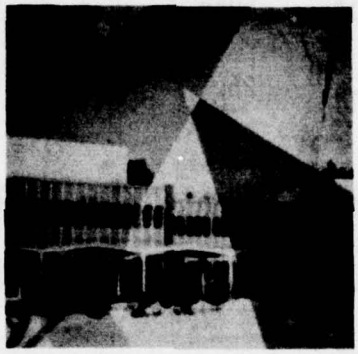

Original with Illumination

Figure 7

Effect of Illumination Process

$$
\begin{array}{ccccccccccc}
 & & & \cdot & & \cdot & & \cdot & & & \\
 & & \cdot & & \cdot & & \cdot & & \cdot & & \\
 & \cdot & & \cdot & & \cdot & & \cdot & & \cdot & \\
\cdot & & \cdot & & h_{22} & & 2h_{02} & & h_{22} & & \cdot \\
 & \cdot & & h_{12} & & h_{11} & & h_{11} & & h_{12} & \\
\cdot & & \cdot & & 2h_{02} & & 4h_{00} & & 2h_{02} & & \cdot \\
 & \cdot & & h_{12} & & h_{11} & & h_{11} & & h_{12} & \\
\cdot & & \cdot & & h_{22} & & 2h_{02} & & h_{22} & & \cdot \\
 & \cdot & & \cdot & & \cdot & & \cdot & & \cdot & \\
 & & \cdot & & \cdot & & \cdot & & \cdot & &
\end{array}
$$

Figure 8

Point Spread Function of Composite Filter

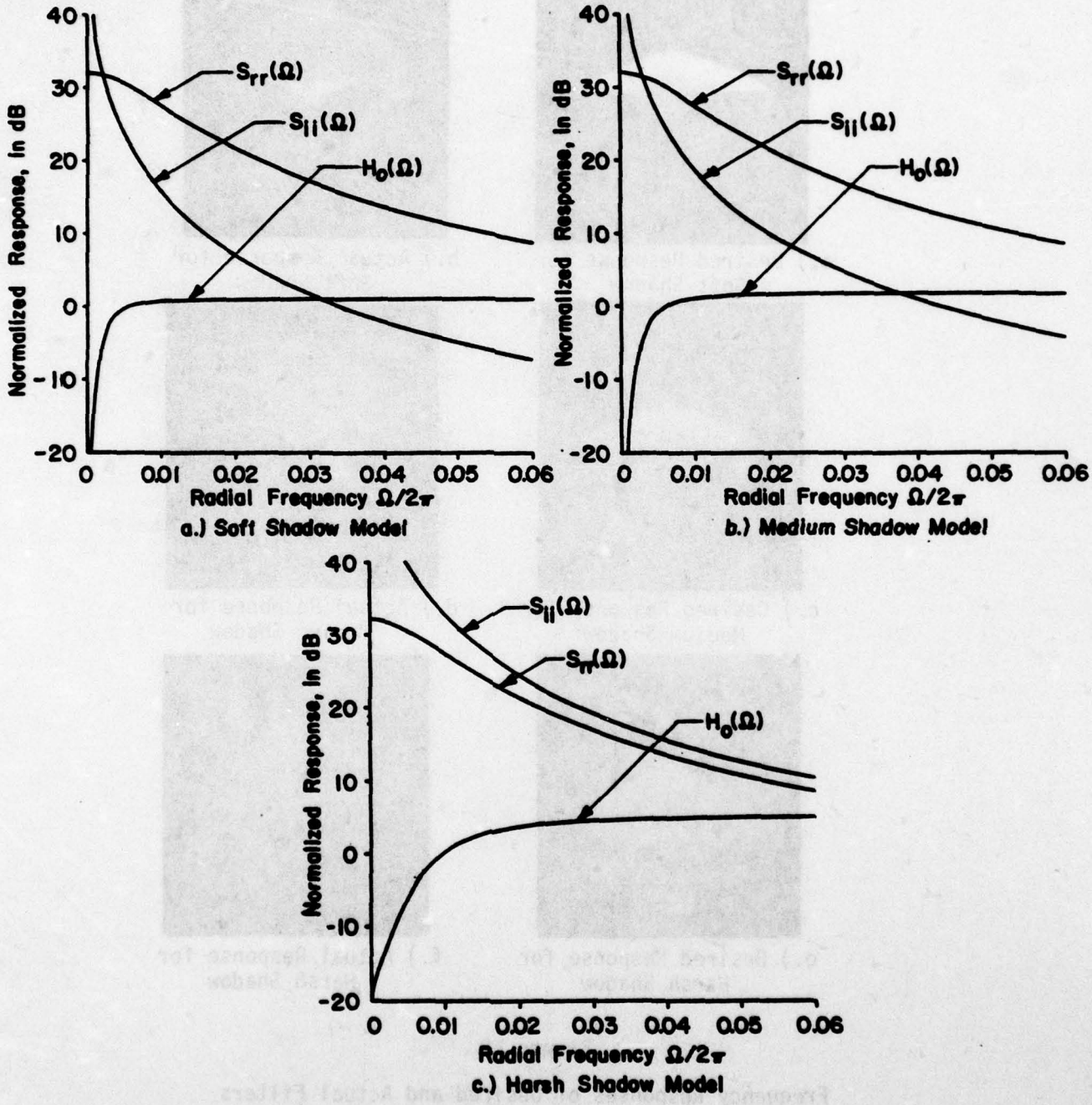

Figure 9
Illustration of Typical Power Spectral
Densities and Associated
Wiener Filter Response

a.) Desired Response for Soft Shadow

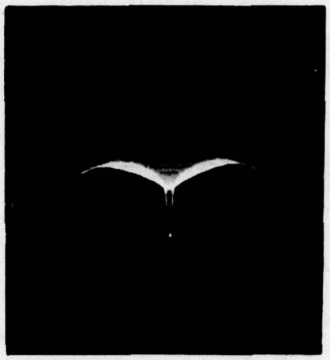

b.) Actual Response for Soft Shadow

c.) Desired Response for Medium Shadow

d.) Actual Response for Medium Shadow

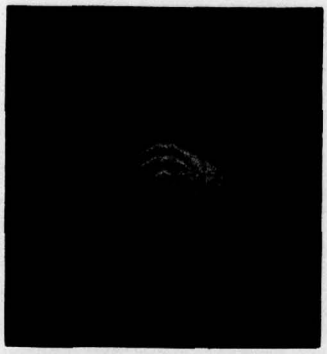

e.) Desired Response for Harsh Shadow

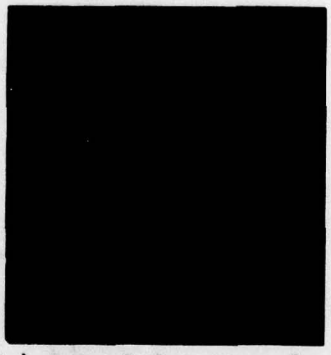

f.) Actual Response for Harsh Shadow

Figure 10

Frequency Responses of Desired and Actual Filters

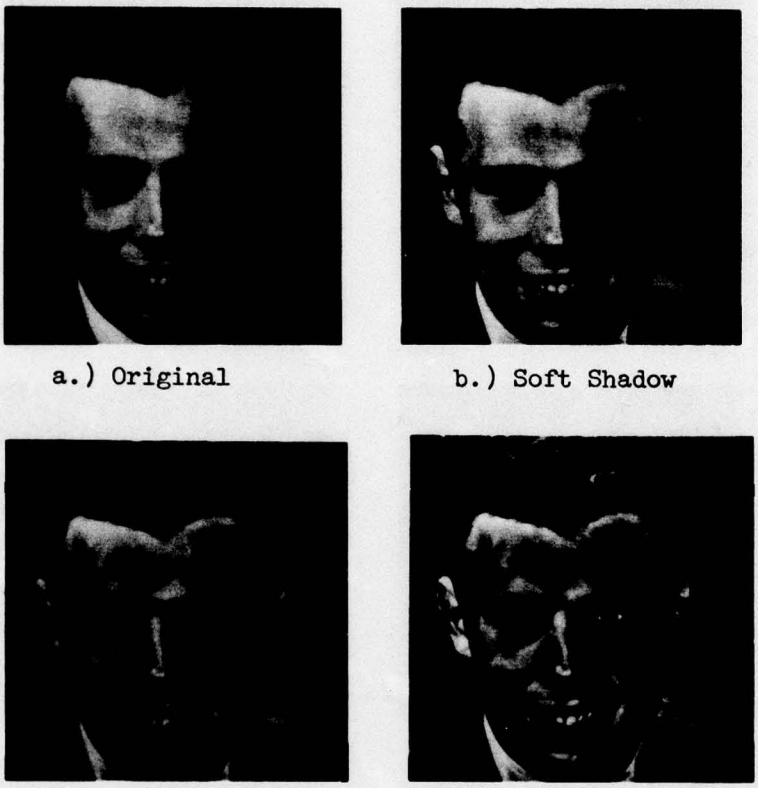

a.) Original

b.) Soft Shadow

c.) Medium Shadow

d.) Harsh Shadow

Figure 11

Typical Results on Head-and-Shoulder Image

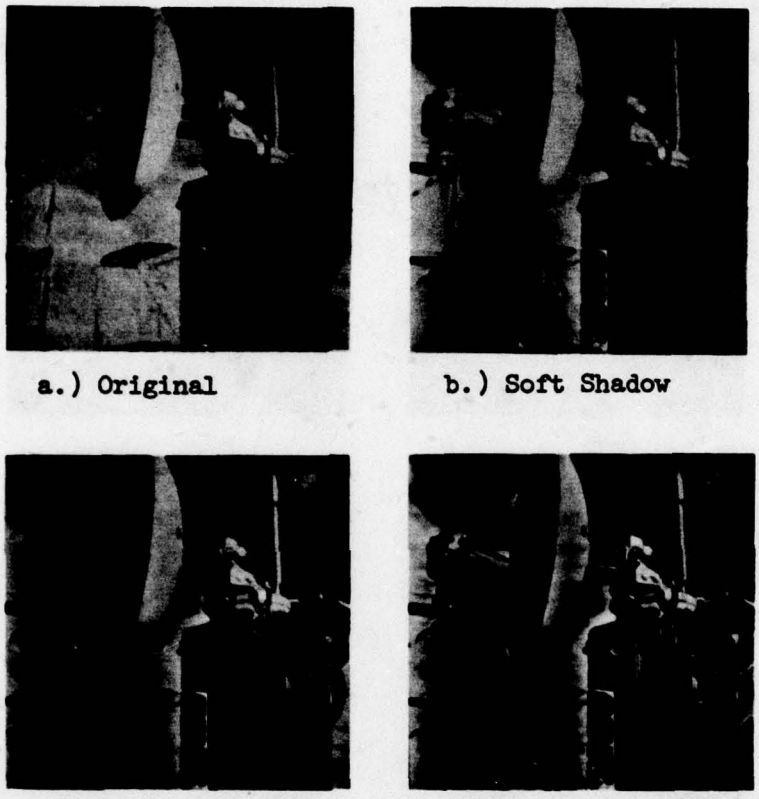

a.) Original b.) Soft Shadow

c.) Medium Shadow d.) Harsh Shadow

Figure 12

Typical Results on Outdoor Scene

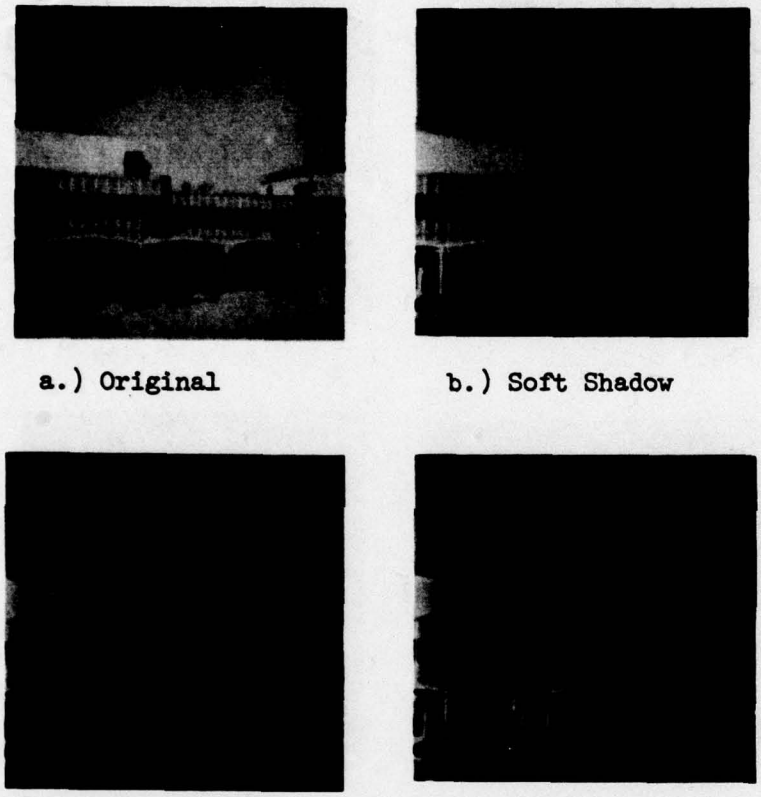

a.) Original b.) Soft Shadow

c.) Medium Shadow d.) Harsh Shadow

Figure 13

Typical Results on Building Image

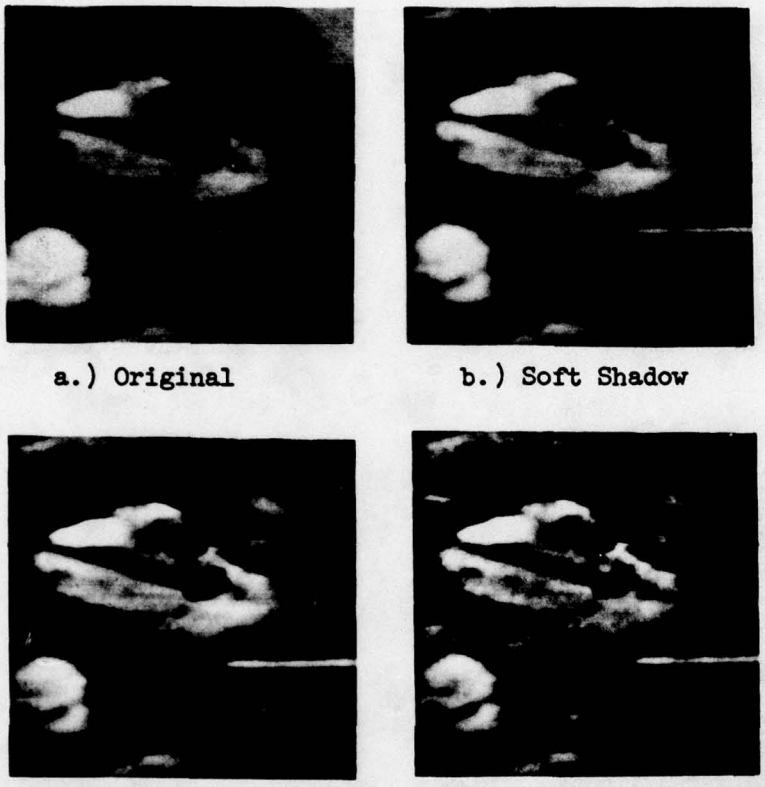

a.) Original b.) Soft Shadow

c.) Medium Shadow d.) Harsh Shadow

Figure 14

Typical Results on FLIR Image

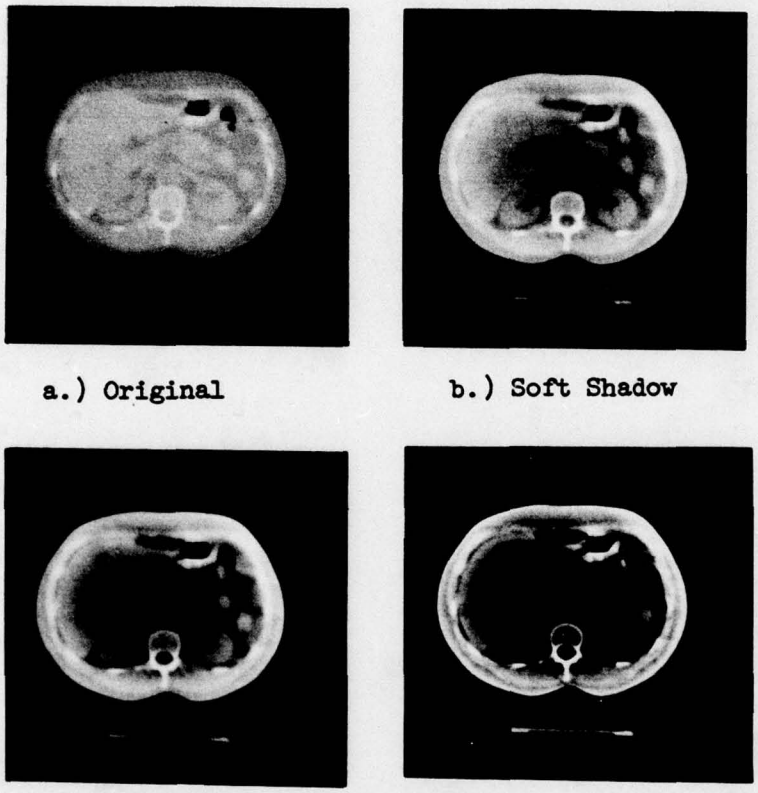

a.) Original b.) Soft Shadow

c.) Medium Shadow d.) Harsh Shadow

Figure 15

Typical Results on Tomograph

DISTRIBUTION LIST FOR ONR ELECTRONIC
AND SOLID STATE SCIENCES

Director — 1 copy
Advanced Research Projects Agency
Attn: Technical Library
1400 Wilson Boulevard
Arlington, Virginia 22209

Office of Naval Research — 1 copy
Electronics Program Office (Code 427)
800 North Quincy Street
Arlington, Virginia 22217

Office of Naval Research — 6 copies
Code 105
800 North Quincy Street
Arlington, Virginia 22217

Director
Naval Research Laboratory
455 Overlook Avenue, S.W.
Washington, D. C. 20375
Attn: Technical Library — 6 copies
Code 5200 — 1 copy
5210 — 1 copy
5270 — 1 copy
6400 — 1 copy

Office of the Director of Defense — 1 copy
Research and Engineering
Information Office Library Branch
The Pentagon
Washington, D. C. 20301

Defense Documentation Center — 12 copies
Cameron Station
Alexandria, Virginia 22314

Commanding Officer — 1 copy
Office of Naval Research Branch Office
536 South Clark Street
Chicago, Illinois 60605

San Francisco Area Office — 1 copy
Office of Naval Research
50 Fell Street
San Francisco, California 94102

Commanding Officer — 1 copy
Office of Naval Research Branch Office
1030 East Green Street
Pasadena, California 91101

Commanding Officer — 1 copy
Office of Naval Research Branch Office
495 Summer Street
Boston, Massachusetts 02210

New York Area Office — 1 copy
Office of Naval Research
715 Broadway, 5th Floor
New York, New York 10003

ODDR&E Advisory Group on Electron Devices — 1 copy
201 Varick Street
New York, New York 10014

Naval Air Development Center — 1 copy
Attn: Technical Library
Johnsville
Warminster, Pennsylvania 18974

Naval Weapons Center
China Lake, California 93555
Attn: Technical Library — 1 copy
Code 6010 — 1 copy

Naval Research Laboratory — 1 copy
Underwater Sound Reference Division
Technical Library
P. O. Box 8337
Orlando, Florida 32806

Navy Underwater Sound Laboratory — 1 copy
Technical Library
Fort Trumbull
New London, Connecticut 06320

Commandant, Marine Corps — 1 copy
Scientific Advisor (Code AX)
Washington, D. C. 20380

Naval Ordinance Station — 1 copy
Technical Library
Indian Head, Maryland 20640

Naval Postgraduate School
Monterey, California 93940
Attn: Technical Library — 1 copy
Electrical Engineering Department — 1 copy

Naval Missile Center Technical Library (Code 5632.2) Point Mugu, California 93010	1 copy
Naval Electronics Laboratory Center San Diego, California	
Attn: Technical Library	1 copy
Code 2300	1 copy
2600	1 copy
4800	1 copy
Naval Undersea Warfare Center Technical Library 3202 East Foothill Boulevard Pasadena, California 91107	1 copy
Naval Weapons Laboratory Technical Library Dahlgren, Virginia 22448	1 copy
Naval Ship Research and Development Center Central Library Code L42 and L43) Washington, D. C. 20007	1 copy
Naval Surface Weapons Center White Oak Laboratory Silver Spring, Maryland 20910	
Attn: Technical Library	1 copy
Code 200	1 copy
212	1 copy
Deputy Chief of Naval Operations (Development) Technical Analysis and Advisory Group (Code NOP-077D) Washington, D. C. 20350	1 copy
Commander Naval Air Systems Command Washington, D. C.	
Attn: Code 310	1 copy
360	1 copy
Commander Naval Electronics Systems Command Washington, D. C. 20360	
Attn: Code 304	1 copy
310	1 copy
Commander Naval Sea Systems Command Washington, D. C. 20360	1 copy
Naval Surface Weapons Center Attn: Library Dahlgren, Virginia 22448	1 copy

Air Force Office of Scientific Research — 1 copy
Attn: Electronic and Solid State Sciences Division
Department of the Air Force
Washington, D. C. 20333

Air Force Weapon Laboratory — 1 copy
Technical Library
Kirtland Air Force Base
Albuquerque, New Mexico 87117

Air Force Avionics Laboratory — 1 copy
Air Force Systems Command
Technical Library
Wright-Patterson Air Force Base
Dayton, Ohio 45433

Air Force Cambridge Research Laboratory — 1 copy
L. G. Hanscom Field
Technical Library
Cambridge, Massachusetts 02138

Harry Diamond Laboratories — 1 copy
Technical Library
Connecticut Avenue at Van Ness, N. W.
Washington, D. C. 20438

U. S. Army Research Office — 1 copy
Box CM, Duke Station
Durham, North Carolina 27706

Director — 1 copy
U. S. Army Engineering Research
and Development Laboratories
Fort Belvoir, Virginia 22060
Attn: Technical Documents Center

Director National Bureau of Standards — 1 copy
Attn: Technical Library
Washington, D. C. 20234

Superintendent — 1 copy
Materials Sciences Division
Naval Research Laboratory
4555 Overlook Avenue S.W.
Washington, D.C. 20375

SUPPLEMENTAL LIST FOR SYSTEMS AREA

Office of Naval Research — 2 copies
800 N. Quincy Street
Arlington, Virginia 22217
Attn: Code 430

Naval Research Laboratory — 1 copy
4555 Overlook Avenue, S. W.
Washington, D. C. 20375
Attn: Code 5400

Naval Electronics Laboratory Center
San Diego, California 92152
Attn: Code 3000 — 1 copy
5000 — 1 copy
5600 — 1 copy

Air Force Office of Scientific Research — 1 copy
Mathematical and Information Sciences Directorate
1400 Wilson Blvd.
Washington, D. C. 20333

Unclassified

SECURITY CLASSIFICATION OF THIS PAGE (When Data Entered)

REPORT DOCUMENTATION PAGE	READ INSTRUCTIONS BEFORE COMPLETING FORM
1. REPORT NUMBER (14) TR-79-2 ✓	2. GOVT ACCESSION NO.
3. RECIPIENT'S CATALOG NUMBER	
4. TITLE (and Subtitle) (6) IMAGE ENHANCEMENT BY STOCHASTIC HOMOMORPHIC FILTERING.	5. TYPE OF REPORT & PERIOD COVERED (9) Technical Report.
6. PERFORMING ORG. REPORT NUMBER	
7. AUTHOR(s) (10) R. W. Fries and J. W. Modestino	8. CONTRACT OR GRANT NUMBER(s) (15) N0014-75-C-0281 ✓
9. PERFORMING ORGANIZATION NAME AND ADDRESS Electrical & Systems Engineering Dept. 409 318 ✓ School of Engineering Rensselaer Polytechnic Institute, Troy, N.Y. 12181	10. PROGRAM ELEMENT, PROJECT, TASK AREA & WORK UNIT NUMBERS NR 375-971
11. CONTROLLING OFFICE NAME AND ADDRESS Dept. of the Navy, Office of Naval Research (11) Electronic & Solid State Sciences Program Arlington, VA 22217	12. REPORT DATE February 1979
	13. NUMBER OF PAGES 37
14. MONITORING AGENCY NAME & ADDRESS (if different from Controlling Office) 401 653 (12) 47 p.	15. SECURITY CLASS. (of this report)
	15a. DECLASSIFICATION/DOWNGRADING SCHEDULE

16. DISTRIBUTION STATEMENT (of this Report)

Distribution unlimited; approved for public release

17. DISTRIBUTION STATEMENT (of the abstract entered in Block 20, if different from Report)

18. SUPPLEMENTARY NOTES

19. KEY WORDS (Continue on reverse side if necessary and identify by block number)

Image Processing, Image Enhancement, Homomorphic Filtering, Least Mean-Square Spatial Filtering

20. ABSTRACT (Continue on reverse side if necessary and identify by block number)

The problem of image enhancement by nonlinear two-dimensional (2-D) homomorphic filtering is approached using stochastic models of the signal and degradations. Homomorphic filtering has been used previously for image enhancement but the linear filtering operation has generally been chosen heuristically. In this paper stochastic image models described and analyzed previously by the authors are used to model the true image and interferring components (shadows and salt-and-pepper noise). The problem of designing the linear operation can then be formulated as one of linear least mean-squared error (Wiener) filtering.

→ next page

DD FORM 1 JAN 73 1473 EDITION OF 1 NOV 65 IS OBSOLETE S/N 0102-014-6601

Unclassified

SECURITY CLASSIFICATION OF THIS PAGE (When Data Entered)

409 238

slt

Examples of processing on typical real-world images are included to indicate the results obtainable.